




UAV-Based Photogrammetry and LiDAR for the Characterization of Ice Morphology Evolution

Teng Li , Baogang Zhang, Wen Xiao , Xiao Cheng, Zhenhong Li , *Senior Member, IEEE*, and Jian Zhao

Abstract—Ice doline is a particular kind of ice morphology, usually scattered on ice streams which are mostly far from the existing research bases. For this reason, glaciologists rarely have opportunities to document its developments in detail. Satellite observations are too coarse to capture such fine features, whereas unmanned aerial vehicle (UAV)-based structure-from-motion (SfM) and light detection and ranging (LiDAR) technologies have revolutionized geosciences research, especially in less accessed polar regions. We developed two bespoke UAV systems for glaciological investigation and carried out four campaigns during two consecutive Chinese Antarctic expeditions in 2017 and 2018. Founded on manual co-registration and accuracy assessment, a successful application to characterize a doline's spatio-temporal evolution is presented in this article. The overlying weight of surface melting directly triggered the collapse event on Jan 30, 2017 near the *Dalk Glacier*, and then the newborn doline grew for another 8135.6 m² in area and 280 303.38 m³ in volume by early 2018. The UAV-based results revealed the doline's changes during a year, showing a maximum horizontal extension of 50 m and vertical subsidence of more than 10 m. Furthermore, we evaluate the photogrammetry and LiDAR systems and find the former is cost-effective and time-efficient on a large-scale survey, while the latter enjoys a better capability to characterize ice morphological details. Based on systematic comparisons, other pros and cons of the two techniques are discussed. To achieve the best performance for relevant applications in similar scenarios, we recommend adopting an integrated approach, in which the LiDAR restores the fine features on the basis of extensive SfM coverage.

Index Terms—Antarctica, change detection, digital elevation model (DEM), ice doline, light detection and ranging (LiDAR), structure-from-motion (SfM), unmanned aerial vehicle (UAV).

I. INTRODUCTION

ICESCAPE is an area covered with ice or ice formations, usually with a particular combination of glacial morphological structures. These features can manifest on ice surfaces across various spatial scales, including melting runoff, supraglacial lake, crevasse, longitudinal strip, doline, moulin, moraine, etc. [1]. The ice morphology is constantly transforming in response to the thermal and stress regime of the past and present continuum dynamics. Due to the aggravated global warming and iconic climate change during the last decades, drastic and profound transitions are observed in the Antarctic ice sheet, especially around the coastal zone [2]. Satellite remote sensing often serves as an efficient way for continent-wide mapping projects, but it remains a challenge for glaciologists to resolve fine-scale features from space.

Recent advances in unmanned aerial vehicle (UAV) systems open up new opportunities for researchers in the cryosphere community [3]–[6]. As an intermediate platform of data collection, UAVs offer a flexible compromise between high spatial resolution and broad spatial coverage, and therefore fill the gap between satellite observations and in-field measurements [7]. Together with structure-from-motion (SfM) technique, they have demonstrated excellent performance even in harsh environmental conditions of polar regions, such as strong winds, low temperatures, weak illumination, and geomagnetic anomaly [8]. On an appropriate scale, the applications of UAVs cover across multiple disciplines related to cold environments, such as albedo measurement [9], sea-ice characterization [10], navigation over polar ocean [11], snowpack property estimation [12], penguin counting [13], and vegetation ecology [14]. A UAV platform could also mount sounding radar to probe fine-resolution basal topography in the West Antarctic ice sheet [15]. In terms of glaciology and ice morphology, the vertical take-off and landing (VTOL) UAV was proved to be effective in capturing the short-lived speed-up event and the subaerial melting hydrology [16]. In another case in West Greenland, the orthomosaic product from UAV collections was utilized to delineate multiple structural features, including crevasse traces, debris covers, supraglacial channels, and flowlines [17].

Light detection and ranging (LiDAR), based on either terrestrial (TLS) or airborne (ALS, including UAV) laser scanning system, is another technology broadly applied to glacial

Manuscript received May 9, 2020; revised July 6, 2020; accepted July 14, 2020. Date of publication July 17, 2020; date of current version August 3, 2020. This work was supported in part by the National Natural Science Foundation of China under Grant 41830536, Grant 41925027, and Grant 41676182, in part by the Chinese Polar Environment Comprehensive Investigation and Assessment Program, and in part by the UK NERC SHEAR Project: WeACT (NE/S005919/1). The work of T. Li was supported by the CSC UK-China Joint Research and Innovation Partnership Fund Ph.D. Placement Program. (*Corresponding author: Xiao Cheng.*)

Teng Li, Baogang Zhang, and Jian Zhao are with the College of Global Change and Earth System Science (GCESS), State Key Laboratory of Remote Sensing Science, Beijing Normal University, and University Corporation for Polar Research (UCPR), Beijing 100875, China (e-mail: congratulation1992@163.com; zhang_bob@bnu.edu.cn; zhaojian@bnu.edu.cn).

Wen Xiao is with the School of Engineering, Newcastle University, NE1 7RU Newcastle Upon Tyne, U.K. (e-mail: wen.xiao@newcastle.ac.uk).

Xiao Cheng is with the School of Geospatial Engineering and Science, Southern Marine Science and Engineering Guangdong Laboratory, Sun Yat-Sen University, Zhuhai 519082, China, and also with the University Corporation for Polar Research (UCPR), Beijing 100875, China (e-mail: chengxiao9@mail.sysu.edu.cn).

Zhenhong Li is with the School of Engineering, Newcastle University, NE1 7RU Newcastle Upon Tyne, U.K., and also with the College of Geological Engineering and Geomatics, Chang'an University, Xian 710054, China (e-mail: zhenhong.li@newcastle.ac.uk).

This article has supplementary downloadable material available at <http://ieeexplore.ieee.org>, provided by the authors.

Digital Object Identifier 10.1109/JSTARS.2020.3010069

landform extraction [18]. With the capability of capturing three-dimensional features actively, it enables producing digital terrain model (DTM) in adverse environments, e.g., low-light conditions. Coordinated with synchronous Global Navigation Satellite System (GNSS) precise positioning stations, LiDAR could reach up to centimeter-level accuracy and even finer resolution [19]. There are already considerable successful case-studies using LiDAR for quantitative glacial terrain analyses and dynamic modeling, such as calving volume calculation [20], paleo-glacial features identification [21], and para-glacial slope monitoring [22]. However, rare work directly targets on the ice morphology. For example, a suite of sensor package, including a camera and a LiDAR unit, was designed to map the ice topography and surface roughness by the University of Colorado. The elevation accuracy was found less than 10 cm after three successful tests in Greenland, Svalbard, and the Southern Ocean, respectively [23]. Recently, Huang *et al.* [24] developed an effective algorithm to extract crevasse features from airborne LiDAR point clouds.

Ice doline (or ice caldera) is a unique surface slumping morphology on fast ice streams. Dr. F. Loewe first borrowed this terminology from Karst landform to describe such catastrophic collapse in the glaciated region. Thereafter, Mellor gave a formal definition [25]. He ascribed the depressions to the “collapse of the surface ice after bodies of englacial water are drained”. Then, Moore drew an analogy from the ice blister and pointed out the similarities and differences between those two phenomena [26]. More cases were found later in the convergence zone of the *Lambert Glacier* drainage system [27], which implied the intimate interactions between the ice doline and glacial flow dynamics. Thanks to the development of very high-resolution (VHR) optical satellite since the twenty-first century, Bind-schadler elaborated a formation theory with the help of VHR IKONOS imagery [28]. However, none of the above work has the opportunity to model the doline’s dynamic process. Although some features containing significant implications for glacial dynamics have been found, little information about their formation and evolution has been acquired by now, mainly because of the inaccessibility of their locations for safety reasons. On Jan 30, 2017, a catastrophic subsidence event occurred unexpectedly near the *Progress Station* of Russia, in East Antarctica [29]. This nascent doline was discovered by the Chinese expedition team, offering a valuable chance to closely monitor its development mechanism.

There is extensive literature on UAV-based SfM or LiDAR applications in terrain morphological analysis. To guarantee the data quality, surveyors normally select ground control points (GCPs) from either existing topographic map [8] or *in situ* measurements [30]. Alternatively, no GCPs geo-referencing approaches begin to emerge when conditions are limited [10], [31]. For multitemporal studies, it is a common practice to measure the shifts of two bedrock areas on each side of the glaciers between multiple surveying products as the uncertainty of DEM differentiation [32]. In this article, based on the orthomosaics and elevation models from the two UAV technologies, we make full use of the well-established DEM of difference (DoD) methodology [33] to unravel and quantify the evolution of ice morphology. To our best knowledge, our datasets characterize a doline’s

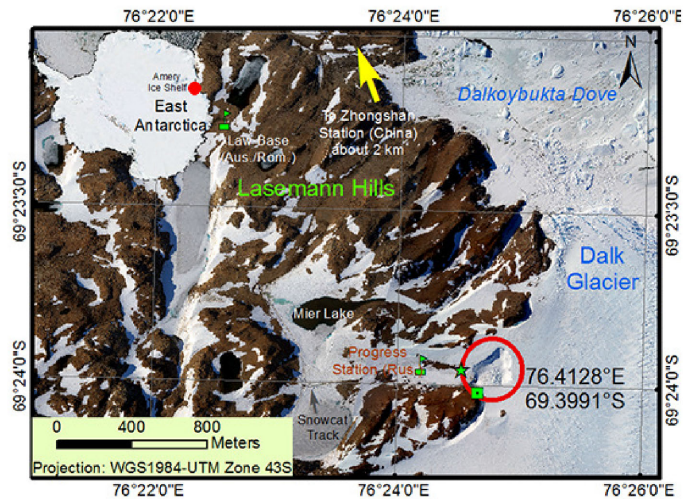


Fig. 1. Environment settings of the study site (main). The Orthomosaic of *Larsemann Hills* and *Dalk Glacier* western front with the collapsed doline and nearby research stations highlighted. The green pentagram and square indicate the location of the operator and navigator during the LiDAR data collection (inset). The geographical location of (main) in the Antarctic continent.

interannual change on a centimeter scale for the first time. Moreover, this study is of practical interest since its future growth might threaten the stability of neighboring research facilities.

II. STUDY SITE

Fig. 1 represents the environment settings of the study area. Surrounded by bare rocks on three sides, the collapse happened in the eastern rim of *Larsemann Hills*, *Ingrid Christensen Coast* East Antarctica, at coordinates of (76.4128°E, 69.3991°S). On the other side, a small tidewater ice stream called *Dalk Glacier* flows northward into the *Dalkoybukta Dove* [34]. Compared with the counterparts scattered on the outlying ice shelf, this doline is easier to access since it is only 300 m from the nearest logistics camp, *Progress Station* of Russia. A little farther away locates the *Law Base* (temporally co-operated by Australia and Romania) and *ZhongShan Station* of China. Before the collapse, this area is frequently crushed by heavy snowcats, hence the track is distinct on snow and ice surface (see Figs. 1). The monthly mean air temperature here is about 0.3 °C in January [35].

III. METHODOLOGY

A. UAV Systems

To test both photogrammetric SfM and LiDAR techniques, we deployed two UAV systems, both low-cost and easy-to-use. The first one is a fixed-wing UAV called *Polar Hawk*, with a wingspan of 1.6 m and a weight of 3.3 kg, mounted with a full-frame SONY DSC-RX1R II camera, and linked to a ground station by radio communication. The expected flying path is preprogrammed using a flight-planning software and is controlled by autopilot after launching by hand. Special aerodynamic designing offers this vehicle a strong wind-resisting capability. The system is the workhorse for operational glaciological investigation program

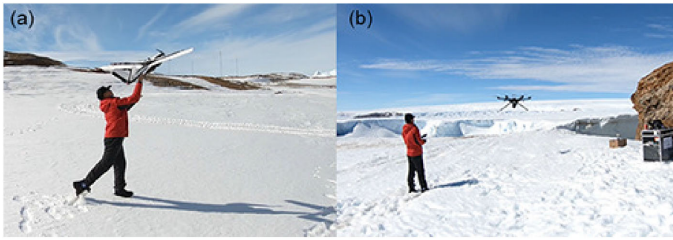


Fig. 2. *In situ* photo of the work scene. (a) Launching Polar Hawk. (b) The Polar Elf taking-off.

of the Chinese National Antarctic Scientific Research Expedition (CHINARE). More information on such system can be found in our preceding publication [10].

The other newly developed system is a customized system called *Polar Elf*. Integrated with off-the-shelf components, it consists of the DJI Matrice-Pro 600 (M600) hexacopter, Velodyne VLP-16 laser scanner, and MEMS Inertial Measurement Unit (IMU). DJI M600 was chosen for its reliable performance in various adverse scenarios. It can hover for about 30 min with the scanner and IMU installed, which is desirable for a small-to-medium investigation project like the one in this article. It is worth noting that the scanner has an independent power and control system, thus M600 acts merely as a mounting platform. The scanning angle is $\pm 15^\circ$ vertically and 360° horizontally [36]. Equipped with a dual-frequency GNSS receiver, the system could collect data at a measurement rate of $300\,000\text{ pt s}^{-1}$, in centimeter-level accuracy. See Fig. 2 and Table I for the UAV systems and their respective parameters.

B. Data Acquisition

Fig. 3 gives an overview of the data acquisition, processing, and analysis. A series of flights were conducted during the 33rd (2016–2017 austral summer) and 34th (2017–2018 austral summer) CHINARE, as a side-project of the operational monitoring program of *Dalk Glacier*. Here in Table II, we list four data collection records. The first one was conducted before the event as an operational glacier monitoring mission, and the second with relatively low flight height was specially designed for capturing the collapse on the immediate next day after the event. According to the imaging geometry, the height scaled the grounding sampling distance (GSD) to 10 cm and 6 cm over average and flat regions, respectively.

To assess the doline's evolution after one year, two following acquisitions were undertaken in the next expedition season, the latter of which was by the UAV-LiDAR system. All operations were carried out in clear-sky or slight cloudy weather conditions, but the sun elevation angle varied, which might challenge the following co-registration between the final products.

During the acquisition of LiDAR data, the pilot manually operated the hexacopter on the west side ($\sim 55\text{ m}$, the pentagram in Figs. 1 and 4), collaborating with an observer standing on the southwest cliff for navigation ($\sim 80\text{ m}$, the square in Figs. 1 and 4).

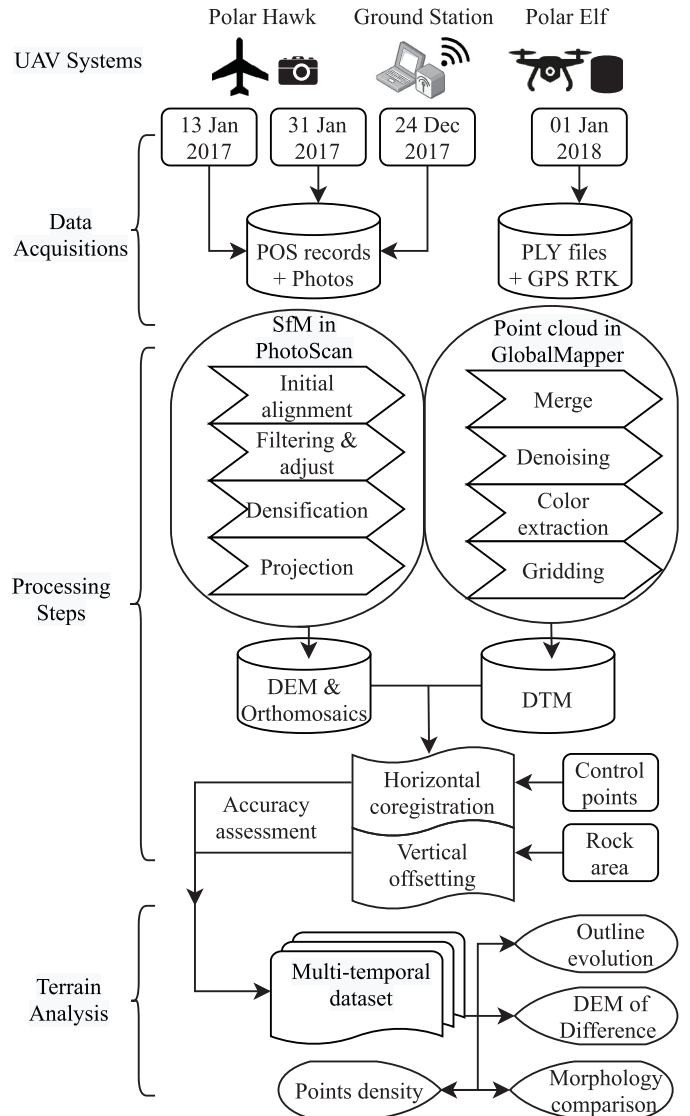


Fig. 3. Diagram of the whole workflow.

C. Data Processing

To process the photos and position and orientation system (POS) records collected by the *Polar Hawk*, we employed the well-known SfM approach in PhotoScan V1.2.4 [37], [38]. This software implements SfM by matching feature points extracted from each photo. Some homogeneous areas with fresh snow may lack surface features and consequently causing blunders in the sparse clouds after initial alignment; therefore, we rejected them and readjusted the image network before densification. The final products of the 10-cm orthomosaic and DEM were exported into the WGS84-UTM43S projection (EPSG: 32743). Based on our previous experiment of Monte-Carlo simulation, the less accurate POS records, especially Z value and yaw angle, dominate the nonlinear georeferencing errors while internal matching retains robust [10].

For point clouds collected by *Polar Elf*, the raw data were referenced by a GNSS base station using real-time kinematic

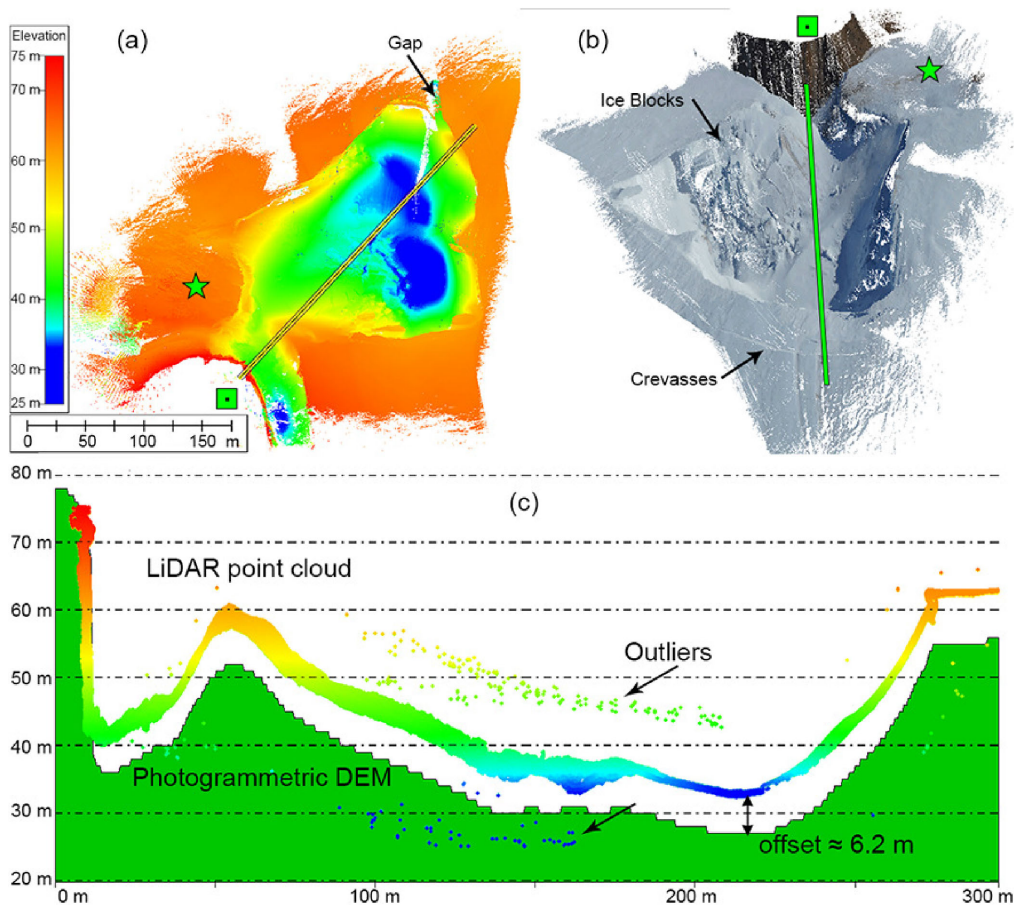


Fig. 4. Raw point clouds of the collapsed ice doline. The indications of the green pentagram and square are the same as in Fig. 1. (a) Plain view. (b) 3-D view, rendered by RGB color from the recent orthomosaic. (c) Elevation profile of the green line in (a) and (b) before eliminating the vertical offset. The point clouds share the same color scheme with (a).

(RTK) technique, and then stored in the polygon (PLY) format. After applying ICP (iterative closest point) registration to each point cloud pairs, we merged multiple *.ply files into a single LAS file in CloudComapre V2.10 but still found a little mismatch among them. First, any points out of the range 25–75 m were excluded after exploratory profiling transects across multiple directions [see Fig. 4(c)] in GlobalMapper V18.0. Then, the default denoising tool in the software was adopted to filter out any rest outliers, after which 112 904 815 points out of 115 557 942 were left for DTM derivation. In the end, to make it comparable to SfM products, a DTM raster with a resolution of 10 cm was generated by gridding the (auto-classified) ground points.

Since the *Polar Hawk* system was not coordinated with precise positioning base station at that time, the POS records can only rely on onboard GNSS receiver and IMU, which may suffer from low accuracy. For the convenience of the later comparison, we manually co-registered all image products to the orthomosaic of Dec 24, 2017. The co-registration work is essentially a technical challenge due to the land/icescape variations and nonlinear distortion [39]. Due to the ice flow of *Dalk Glacier* on the east side of the doline, we can only find surrounding bare rocks on the other three sides, which inevitably results in nonuniform bias.

A two-step co-registration strategy was adopted, in which we dealt with the horizontal misfit and vertical offset separately. In the first step, for the horizontal misfit, we manually selected 15 well-distributed control points around the collapse (see Fig. 5). Provided the orthomosaics were superimposed perfectly, theoretically, the pixel-based DoD over the corresponding stable areas should be a constant. In the second step, for the vertical offset, we clipped a small rock field close to the northwest doline (see Fig. 5), and then deduced biases and uncertainties based on statistics of the differences between the DEM pairs.

Likewise, we manually co-registered the LiDAR-derived DTM of Jan 1, 2018 with the closest SfM-derived DEM of Dec 24, 2017, but for this case, we had no rock field around in the LiDAR data due to the limited coverage. Assuming little change occurred within just one week, we therefore directly co-registered these two terrain models, based on the cavity edge, ice blocks within the cavity, and morphological features around it. Afterward, we detected a quite large vertical offset between the LiDAR-derived DTM and SfM-derived DEM in a preliminary comparison [see Fig. 4(c)]. Accordingly, a constant value of 6.2 m, which is the average difference between the two profiles, was subtracted from LiDAR to compensate such an undesirable shift. Since the two systems are using two different

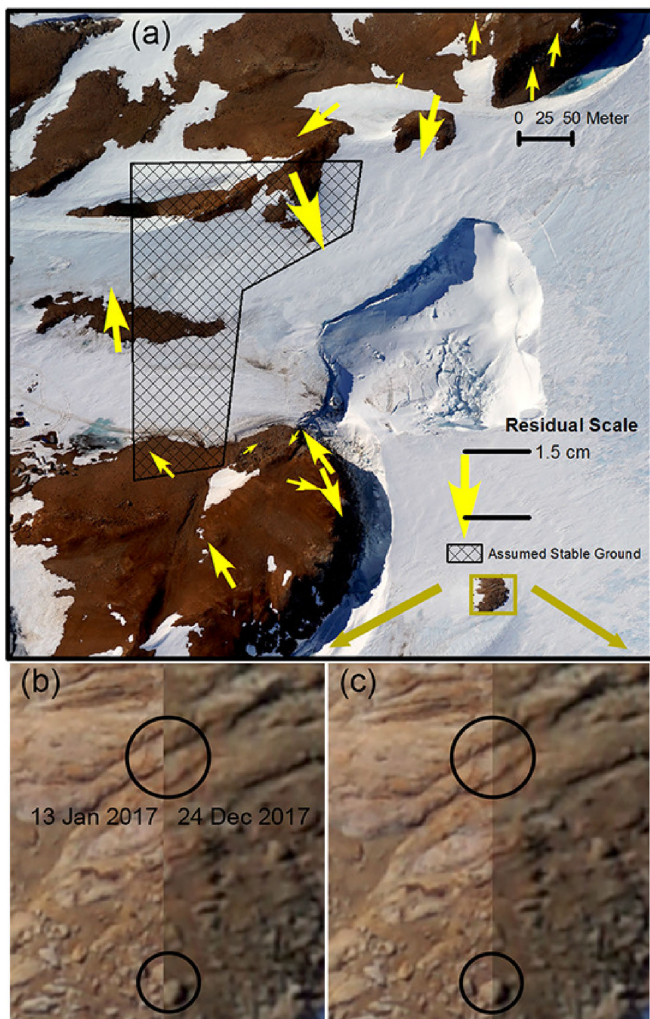


Fig. 5. Co-registration result of Dec 24, 2017 to Jan 13, 2017. (a) Spatial distribution of selected control points, and the assumed stationary area to evaluate the performance. The arrows represent the direction and magnitude of the co-registration residuals, which are from 0.03 pixels (0.3 cm) to 0.25 pixels (2.5 cm). (b) The zoom-in view of the rock field in green box before co-registration. As a qualitative check, no control point was set here. (c) The same configuration as (b) but after co-registration. Note the continuous pattern of rock fractures and isolated boulder in black circles.

sets of position and orientation units, the large offset could account to the accumulation of errors from each of the units. In fact, the multiple photogrammetric acquisitions show relatively consistent products (offset <50 cm), as they are using the same platform. But the absolute georeferencing accuracy remains unknown. In addition, it is suspected that there is not enough time for the GNSS base to precisely resolve the location when collecting LiDAR data. We presume LiDAR data could suffer from a systematic height error from the GNSS base station. Without further information, we could not reach any concrete conclusion. Nevertheless, it is worth noting that the absolute elevation difference between the two types of data has little, if not none, impact on the interdata relative comparison. The Velodyne laser scanner we used is unable to acquire spectral information (only intensity available), we rendered each point via RGB from

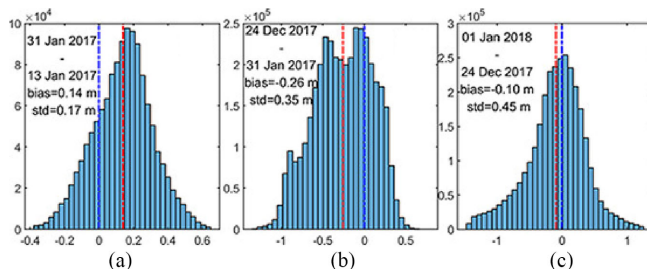


Fig. 6. Histogram of elevation differences of (a) Jan 31, 2017–Jan 13, 2017, in outlying (assumed) stationary rock and snowfield; (b) Dec 24, 2017–Jan 31, 2017, the same area as in (a). Note the bi-modal pattern; (c) Jan 1, 2018–Dec 24, 2017, inside the doline, with all means (bias) and zeroes (no change) value labeled.

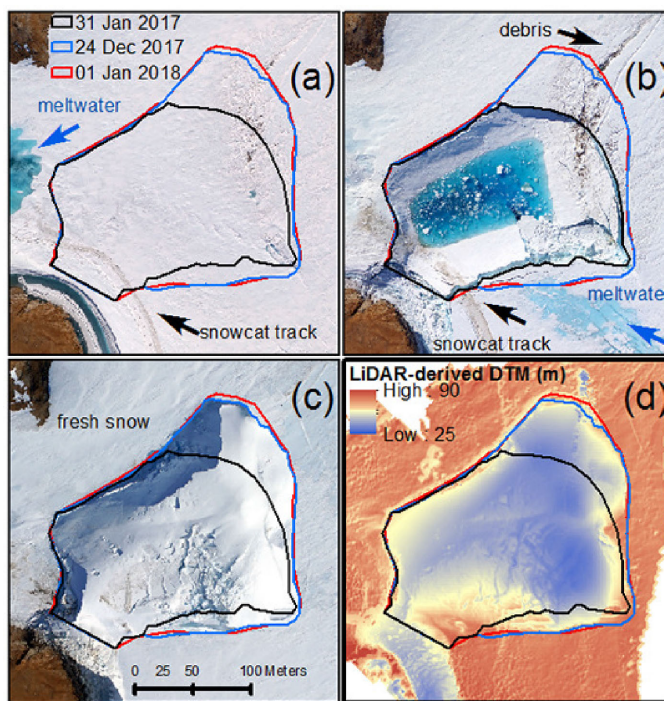


Fig. 7. Spatio-temporal evolution of the doline, with the outlines of different time superimposed on the orthomosaics or DTM. (a) Jan 13, 2017. (b) Jan 31, 2017. (c) Dec 24, 2017. (d) Jan 1, 2018.

the nearest pixel in the orthomosaic of Dec 24, 2017 to create a 3D view [see Fig. 4(b)], after applying the same transformation to filtered point clouds as the DTM co-registration.

Before the formal analysis, we first assess the co-registration accuracy. For the horizontal dimension, the mean absolute deviations (MADs) were calculated over control points residuals after georeferencing. For the vertical dimension, the DoD statistics were evaluated over the motionless area near the doline. To characterize the doline’s formation and evolution, we then delineated the doline’s outline in different dates and recognized varying features from orthomosaics. The DoD within each outline was computed and a profile along the developing direction was sampled to reveal the subsidence trend. To demonstrate the difference between SfM and LiDAR products, we computed the

TABLE I
KEY PARAMETERS OF TWO UAV SYSTEMS

System	Platform	Payload	Weight	Endurance [*]	GNSS	Output	Final product
Polar Hawk	Feima fixed-wing	SONY DSC-RX1R II camera	3.5 kg	90 min	onboard, coarse	photos+POS records	orthomosaic+DEM
Polar Elf	DJI M600	Velodyne VLP-16 LiDAR	11 kg	30 min	RTK, precise	point clouds	DTM

^{*}Depending on air temperature.

TABLE II
DATA COLLECTION RECORDS

Date	System	Flight	Target	Evolution Phase
13 Jan 2017	Polar Hawk	500 m, pre-defined path	Dalk Glacier	Preparing
31 Jan 2017	Polar Hawk	300 m, pre-defined path	Ice Doline	Collapsing
24 Dec 2017	Polar Hawk	500 m, pre-defined path	Dalk Glacier	Developing
01 Jan 2018	Polar Elf	60-80 m, manually navigating	Ice Doline	Stabilized (?)

LiDAR point density by a searching radius of 3 m in the Gaussian kernel and selected three typical scenes in contrast.

IV. RESULT

A. Co-Registration Accuracy and Reliability

A co-registration result of data from Dec 24, 2017 to Jan 13, 2017 is shown in Fig. 5 as an example. Due to the topographic limitation, we can only rely on the rock field in the west part of the ice doline. Therefore, the tilt of the DEM model along the west and east dimension cannot be eliminated even all the residuals are well below one pixel (10 cm). Besides, a small rock patch, which is far from all control points, is shown before and after co-registration as an independent qualitative check. The continuous texture of fractures and boulders (marked in black circles) also indicates the co-registration reliability in the doline area, which is nearer to control points than the checked rock patches. In sum, the MAD is 3.77 cm for the X dimension, 7.85 cm for the Y dimension, and 9.15 cm for the horizontal dimension.

In Fig. 6, we assess the quality of co-registration in Section III-C. It is worth pointing out that outliers beyond $\text{mean} \pm 3 \times \text{standard deviation}$ were rejected iteratively when computing the representative statistics; otherwise, a few outliers can contaminate these values exceptionally [40]. All distributions of the three histograms behave in the form of Gaussian curve, verifying our assumption that after planimetric treatment, the vertical offset within a small and invariable extent should be a constant plus random noise. For differences between SfM-based elevations in Fig. 6(a) and (b), the co-registration of those acquisitions within 3 weeks (Jan 13–Jan 31, 2017) shows better performance than those acquisitions stretching over 11 months (Jan 31–Dec 24, 2017). This could be expected due to the temporal decoherence effect. The distribution spreads wider for Fig. 6(b) mostly because there is a secondary mode of about -0.5 m besides the primary mode of zero, which pulls the mean value to negative. This secondary modal pattern implies there still exist systematic misfits after horizontal co-registration although we do not identify corresponding control points with unreasonably large residuals after further checking. Without additional information, we postulate such errors are propagated

from the poorly defined vehicle height and yaw angle in POS records of Dec 24, 2017 [10].

The largest standard deviation is found in Fig. 6(c), although it has a mean value closest to zero. Note that this histogram of LiDAR and SfM elevation differences is derived from elevations within the doline, which may experience more dynamic behavior than the bare rocks around. Of particular interest is a little negative skewness of such differences, compared with standard Gaussian distribution. We cannot attribute this skewness for sure, to either uncompensated bias of LiDAR measurements or physical downwasting from ablation (or more plausible, a combination of both factors).

In order to get (quasi-)unbiased terrain difference results, we subtracted the mean values of the above histograms from subsidence calculations in the next section and took standard deviations as uncertainty metrics. From the perspective that errors cannot be eliminated, we regard the preceding accuracy as a fairly conservative estimate for a relatively flat ice field, since the results are derived from rough rock field. In fact, as another qualitative indication, the spatial consistency between the point clouds and orthomosaic of Dec 24, 2017 [Fig. 4(b)] lends us more confidence in the procedures mentioned above. Accounting that we care more about relative changes rather than absolute georeferencing, such manipulation should meet our requirement for the following analysis.

B. Formation and Subsequent Evolution

We find the extensive meltwater before the collapse triggered the catastrophic event [see the blue patch in Fig. 7(a)], as exactly what was reported in [29]. Coming from upstream as far as 3 km in the marginal ice sheet, the accumulated meltwater in mid-summer meanders along the west flank of *Dalk Glacier* till *Dalkoybukta Dove*. On the other hand, the local rock field with lower albedo absorbs more heat, and thus weakens the mechanical strength of adjacent ice. Finally, the thin roof cannot support the weight of the fluid. In the field, we heard the noise of water dripping during the data collection. However, Florinsky and Bliakharskii's research concluded that the surface hydrology system was not involved with englacial or subglacial structures [29], which seems to contradict our observation. See Section V for further discussions about future work.

TABLE III
TEMPORAL GROWTH OF THE ICE DOLINE

Date	13 Jan 2017	31 Jan 2017	24 Dec 2017	01 Jan 2018
Area (m ²)	0	24656.3	32154.2	32791.9
Volume (m ³)	-1600.201	-234636.85	-514940.23	-514719.03

The plain-view plot in Fig. 7(a)–(c) shows the initial collapse developed from an oval shape into a trapezoid, with the long base close to the glacier and short base close to the rock. The ponding inside the doline suggests intense surface melting before the collapse. In the last acquisition, the doline extruded farther towards the ocean with little changes taking place on other sides, which corroborates our hypothesis indirectly.

In terms of the vertical dimension, the volume was more than doubled by early 2018. The outlines derived from orthomosaic of Dec 24, 2017 and point clouds of Jan 1, 2018 are almost identical except the northeast corner. The area difference between the blue and red outlines in Fig. 7, which is up to 387 m², can be hardly explained by mis-registration. Instead, we interpret it as a sign of ongoing and active evolution in mid-summer towards the glacier outlet. However, the volume difference is insignificant (Table III), probably due to the interpolation error from the relatively sparse LiDAR points here. Interestingly the original surface was not flat. We resolve a small and negative amount of volume (1600 m³) even before the collapse, meaning that the subsidence may already exert its effect *a priori*.

To quantify the evolution after one year’s timespan, we make a difference between consecutive DEM pairs, also known as DoD in geomorphology literature [33]. In Fig. 8(b), we discern some artifacts in the central part of the doline. Those artifacts might result from the melting pond on Jan 31, 2017 [see Fig. 7(b)]. Water and drifting ice flows could lead to troubles during the SfM processing. Fig. 8(b) reveals a heterogeneous pattern: large subsidence ranging from -10 to -30 m basically occurred in the eastern part. While setting the net surface mass balance as background in the western part, we infer the more complicated alterations experienced in the central cavity arising from a combination of snow accumulation, meltwater drainage, and refreezing process. Comparatively, the small [usually less than 0.5 m as shown in Fig. 8(a) and (b)] and homogeneous vertical discrepancy outside of this doline implies the spatial coherence as a whole between the two datasets (except for the zone of the original gap in LiDAR data). The location of profiles in Fig. 8(c) is the same as in Fig. 4. In the left end which is closer to the control point, the cliff from different dates coincides with each other exactly. However, in the right end, we detect a consistent subsidence trend of 3.09 m with an uncertainty of 0.39 m ($=\sqrt{0.17^2 + 0.35^2}$) considering the error propagation of Fig. 6(a) and (b). Besides, only the red profile expresses “jagged teeth” just after the collapse while the other two ice surfaces are smooth after long-term wind erosion. In other words, on average, the doline subsided about 22.23 m ($=10.28 + 11.95$) since its formation [Fig. 8(d) and (e)].

C. Comparison Between Two Techniques

Fig. 4 illustrates the LiDAR point clouds. Within the cavity, the surface elevation gradually decreases from the west (close

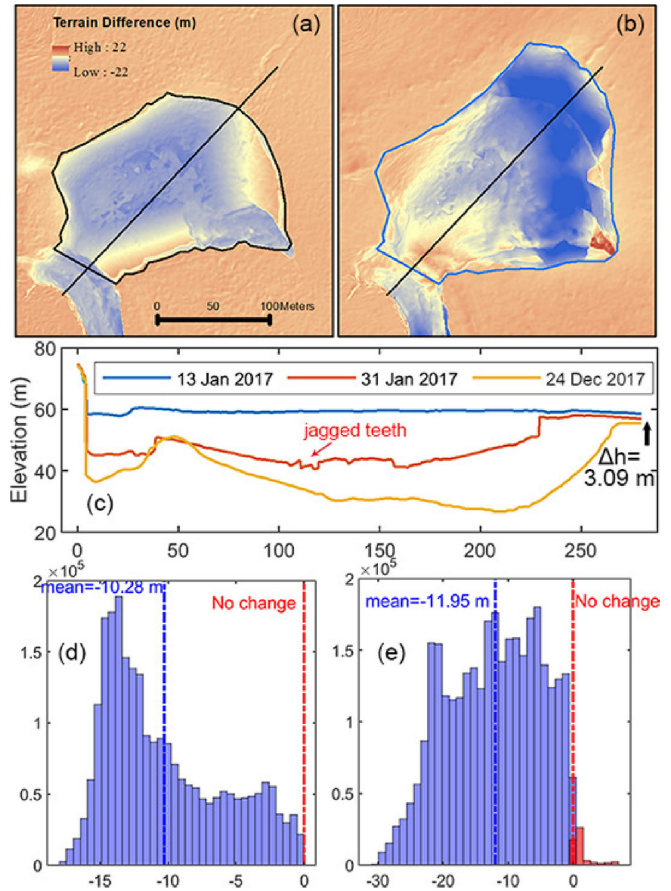


Fig. 8. DoD results, with the negative values for subsidence/erosion and positive for lifting/deposition. (a) Jan 31, 2017–Jan 13, 2017. (b) Dec 24, 2017–Jan 31, 2017. (c) Elevation profiles of the black lines in (a) and (b) from three different dates. (d) Histogram of elevation changes inside the doline in (a). (e) Same configuration as (d) but for (b).

to the rock) to the east (close to the glacier) and reaches its local minimal in two melting depressions. Although small holes still exist along the margin with large gradient or occultation behind the ice blocks, the point clouds capture the holistic topographic variations quite well, especially near the cliff.

Despite the intention to evenly direct the vehicle (and to avoid crush against the cliff at the same time), the overall point distribution is unsatisfying. From Fig. 9, we can recognize the flight paths with high density, between which an obvious yet unrecoverable gap appears at the far-end from the navigator. It is also intuitive to have more returns along the sharp edge and cliff facet to capture details. In general, point density inside the cavity is as high as 1956.86 pt m⁻².

To illustrate the added value of LiDAR data, here in Fig. 10, we pick up two scenes where the SfM method fails to capture the detailed characteristics. The first one is a complex of ice blocks falling from the southern ice slide; the other is a batch of surface crevasses ahead of the extrusion corner. Although LiDAR points were resampled the same as the GSD of photo acquisition (10 cm), for discrete and jumbled blocks, the SfM-derived DEM obscures the topographic relief while the LiDAR-derived DTM expresses clear and definite boundaries. For the other

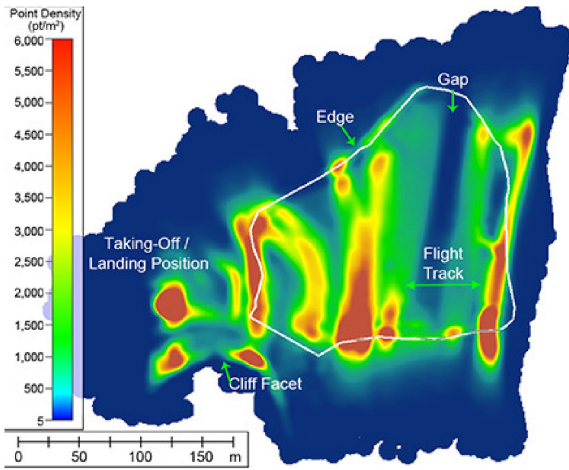


Fig. 9. Density map of point cloud.

case, SfM-derived DEM losses much more information which is critical for logistic safety—the newly developed crevasses, either wide or narrow, are indistinguishable on the subdued surface. Since the dark debris in Fig. 7(b) cannot be seen in Fig. 7(c), the fresh snow conceals the structures necessary for SfM processing. In contrast, the LiDAR-derived DTM explicitly keeps subtle fluctuations despite conspicuous radial distortion in the periphery. In sum, LiDAR data performs better in feature delineation.

Although the general pattern of the results of the SfM-DEM of Dec 24, 2017 and LiDAR-DTM of Jan 1, 2018 is analogous, we move forward to generate the DoD between them to compare the two techniques. We set the minimum level of detection ($_{min}LoD$) as 0.45 m from Fig. 6(c), and maximum one ($_{max}LoD$) as 1 m empirically, out of which we take as gross error. There are two clusters in Fig. 11; one is the shadow area projected by the doline cliff (red circle) and the other is an ice block complex. Such particular spatial patterns remind us the disadvantages of SfM, where this optical passive methodology is less capable of capturing detailed features, due to inappropriate illumination and over-smoothing. Nevertheless, given the clear weather at the end of 2017 and the fact that rough surface could enhance ablation by absorbing more reflected radiance [41], we still regard the subsidence signal is physically rooted, which undermines the previous assumption in co-registration. In other words, the short-term downwasting can be detected by the UAV-derived elevation models if the acquisition geometry is well controlled.

V. DISCUSSIONS

This study contributes to the emerging body of literature regarding geomorphological change analysis based on UAV systems, in arguably one of the most challenging and data-scarce Antarctic fields. Unfortunately, the following data collection campaign was not undertaken in the austral summer during 2018–2019. From the Landsat-8 optical image with 15-m resolution, we do not find prominent variations of this ice doline yet the open satellite remote sensing is too coarse for such small-scale objects. Nevertheless, we would continue the monitoring

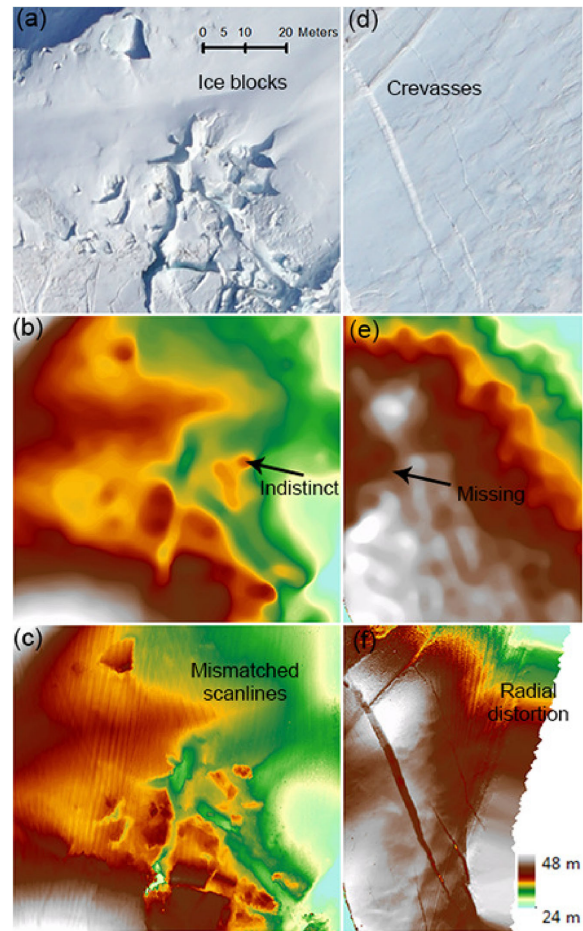


Fig. 10. Added-value of LiDAR beyond the ordinary SfM photogrammetry. Three rows are SfM-derived orthomosaic, SfM-derived DEM, and LiDAR-derived DTM, respectively. Two columns are selected scenes of ice blocks and surface crevasses whose locations are labeled in Fig. 4(b).

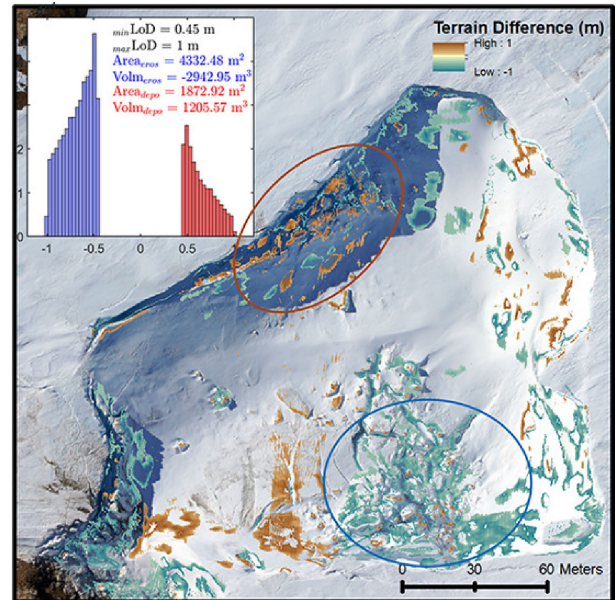


Fig. 11. DoD result of Jan 1, 2018 to Dec 24, 2017, in which LoD was set to a minimum of 0.45 m and a maximum of 1 m. The inset histogram, which is the subset of Fig. 6(c), shows the statistics of erosion and deposition. The red and blue circles represent the shadow and block complex, respectively.

project after 2019 as the applications are granted. Regarding data collection, there are several other limitations in the present study, among which may be the lack of GCPs is in most need of complement. In the preceding work, we have studied the precision characteristics without GCPs [10]. It is no big concern for single-time acquisition, but to some extent, repeated surveys as presented here would necessitate GCPs to overcome the inherent distortion [42]; otherwise, extra care must be taken for manual co-registration before interpreting any physical phenomena.

Exhaustive uncertainty analysis can be difficult on a full error budget basis and is not always necessary [43]. In respect of the processing, we assume the surrounding rock fields are stationary during the acquisition interval [Fig. 6(a) and (b)], which is not necessarily the case. Considering the geomorphic dynamics and varying illumination conditions, rock feature' position can be altered as a result of breaking up and sliding downslope under consistent strong katabatic winds, and a large range of temperature variation, or shifting their shadows under different solar elevations. The same principle also applies to the area inside the doline (Fig. 11), where the ice field can still express thinning via sublimation even if no melting occurs on the surface. As a long-term project, we would deploy artificial GCPs with geodetic accuracy in the next expedition, from which we expect the products to share a common spatial frame. Such efforts would not only relieve the manually co-registration work but also offer an independent and objective quality check.

Another promising direction to reduce the reliance on GCPs comes from the automatic co-registration of multitemporal UAV products. Several researchers have made contributions in alignment with sparse point clouds from unified adjustment blocks containing image chunks from different dates. For example, Li *et al.* proposed to match successive UAV data first before constructing a control point set into a single bundle adjustment processing [44]. Their experiment showed the (relative) accuracy is higher than the traditional method by GCP. Recently, the morphology-based approach was leveraged for landslide detection with almost exclusively image information, namely, "pseudo-control" over stable terrain [45]. They achieved effective co-registration of time-series DEMs derived from a consumer-grade, fixed-wing UAV and SfM pipeline. Similar thoughts were also implemented and formalized into a robust workflow for UAV-based change detection without GCPs [46]. It is worthy of attention that all the above work can only succeed supposing the stable zones are predominant and changes are limited. Whether they are suitable for our research (drastic collapse) remains to be explored in the future. Besides, although the simple 2D differencing of the elevation here accomplishes the terrain evolution monitoring, the DoD on a raster basis might lose detailed information in 3D space. Alternatively, it is not inconceivable that a cloud-to-cloud approach such as the "multiscale model-to-model cloud comparison" (M3C2) algorithm would achieve more insights in some complicated geometry [47], [48].

As illustrated in Fig. 10, the LiDAR system demonstrates great performance in expressing exquisite structures from complex scenes because the derivation is more sensitive to small-scale, locally variable glacial morphology. Nevertheless, as mentioned earlier, we are aware of the high-frequency oscillations

after the merge processing. Such apparent strips emerge as a result of mismatched scanlines on LiDAR-derived DTM, which we attribute to an unstable IMU and GNSS base owing to the limited adjustment time before the actual flight. As a matter of fact, the low temperature in polar regions impairs battery's endurance; therefore, we have to expedite to finish up the LiDAR data collection on Jan 1, 2018. In this aspect, improvements would be made after this testing to enhance the power capability of our newly developed LiDAR model; meanwhile, the data coverage can also be expected to extend farther away from the operator. Beyond the refined characterizing capability, we speculate LiDAR could also partially penetrate through the melting pond, which is very likely the purest water body in natural environment. With that said, LiDAR could be used to sketch shallow water bathymetry in Antarctic [49]. This penetration ability is critical for scenarios like Jan 31, 2017, in which SfM processing suffers from water surface and produces elevation artifacts when matching image features spuriously [see Fig. 7(b)].

On the other hand, UAV-based SfM is advantageous in terms of low cost, less expertise required, and bigger mapping swath. Considering the uncertainty of 0.45 m between the two techniques in Fig. 6, the SfM techniques should be a better choice if refined structures are not required in decent illumination. The submeter accuracy could be adequate in most interannual change detection scenarios. We summarize the strengths, drawbacks, and trade-offs of these two techniques from more perspectives in Table IV. Ideally to reach full merits of both techniques, we advocate a hierarchical strategy for the best practice: the SfM is first employed for large-scale mapping, then complementing particular area of interest by LiDAR before integrating two point clouds together for analysis. We admit a caveat that the viewpoints from such particular study may not be universally applicable in other cases, especially considering the quick advance of hardware and algorithm. The emphasis here is exclusively on ice morphology changes in polar regions.

Our results are consistent with that in Florinsky [29] in terms of the weight of the overlying meltwater straightly breaking down the suspended thin roof. However, we doubt their claim that such a phenomenon had little to do with the subglacial drainage. Instead, the dolines are surface features reflecting basal ice activities [27]. The progress direction towards east also indicates the dominant role of glacier dynamics. From a more comprehensive view, we put forward a number of factors potentially contributing to this event and are working to quantify them based on multidisciplinary datasets: (1) the depressed topography to accumulate meltwater; (2) the concave geometry to drive local air convection; (3) the surrounding rock with low albedo to absorb more solar radiation; (4) the lateral shear stress from the *Dalk Glacier*; (5) the tidal flexure across the grounding zone; and (6) the crush by heavy snowcats repeatedly. Additionally, there are also feedback among those contributors, such as depressed topography that can accumulate meltwater, which, in turn, reduces its local albedo to enhance further melting and lowering. The interactions among above natural and artificial environment factors resulted in the accumulation of water mass here and ultimately leading to the collapse. Verification of the above hypothesis warrants more detailed field work and parameterized investigation on englacial structures.

TABLE IV
COMPARISON OF SfM AND LiDAR DATASETS ACQUIRED BY OUR UAV SYSTEMS

Technique	SfM	LiDAR
Accuracy scale	<1 m	~ 10 cm
Pros	With the corresponding orthomosaic Uniform point clouds distribution Inexpensive in larger spatial extent Easy to plan the flight regardless of small hills An automated workflow in the mature software	True 3D characterization capability Denser point clouds, with mild penetration to subsurface Resolving finer structure or complex geometry Less processing time, flexible comparison Independent of featureless or textually homogeneous fresh snow
Cons	2.5 D characterization for nadir view Coarser point clouds and DEM Insensitive to crevasse features Subject to illumination (shadow, polar night) Computationally intensive to the final product	No corresponding orthomosaic Limited swath and surveying coverage Expensive equipment and longer time to deploy More training and skills to operate Specialized software and experienced interpreter
Integration	SfM for efficiently mapping for gentle topography on large scale, with LiDAR focused on a particular area of interest or complex structures, before compositing two point clouds together for the whole picture meanwhile preserving details.	

VI. CONCLUSION

In this article, we report a UAV application in characterizing ice morphology and its development. The time-series of orthomosaic and elevation models were manually co-registered, and then we adopt a small area of nearby stable rocks to compensate vertical offset and quantify the uncertainty of the DoD. Based on the rectified datasets, the doline formed on Jan 30, 2017 near the *Larsemann Hill* is found to expand from 24 656.3 to 32 791.9 m² in areas, and 234 636.85 to 514 940.23 m³ in volume. We also notice the subsidence signal arouse before the collapse and such cavity sank for another 11.95 ± 0.35 m by Jan 1, 2018. These active changes mainly concentrated in the eastern part, which relieves the concerns about the research infrastructure nearby. The work also provides a good baseline for further research of this ice doline.

In particular, we carried out performance comparison of two UAV-based systems, i.e., photogrammetry and LiDAR. The raw point cloud collected by LiDAR resolves the landform variations with great refinement, especially for chaotic and delicate scenes. It is superior to the widely used UAV-SfM method since the photogrammetry result smooths out too many morphological details. For both SfM and LiDAR, the UAV-based remote sensing platform serves as a valuable tool to facilitate sophisticated geomorphometric interpretation, but which one should be employed depends on the aimed accuracy, surveying coverage, financial support, and operation environment. In sum, for ice morphology characterization, we advocate a hierarchical strategy: the SfM is first employed for large-scale mapping, and then LiDAR is supplemented in areas of particular interest; in the end, the point clouds, surface models, and orthomosaics are integrated for physical analysis.

ACKNOWLEDGMENT

The authors would like to thank Engineers from Yueqian Company, Ltd. and Feima Robotics for technology support. T. Li expresses gratitude to Prof. Hilmar Gudmundsson for hosting him in Newcastle, U.K. The authors also appreciate two anonymous reviewers' and the editor's constructive suggestions to improve the original manuscript.

REFERENCES

- [1] D. Benn and D. J. Evans, *Glaciers and Glaciation*, 2nd ed. Abingdon, U.K.: Routledge, Jun. 2010.
- [2] Y. Liu *et al.*, "Ocean-driven thinning enhances iceberg calving and retreat of antarctic ice shelves," *Proc. Nat. Acad. Sci.*, vol. 112, no. 11, pp. 3263–3268, Mar. 2015.
- [3] S. Higashino, M. Funaki, N. Hirasawa, M. Hayashi, and S. Nagasaki, *Development and Operational Experiences of UAVs for Scientific Research in Antarctica*. Tokyo, Japan: Springer, Mar. 2013, ch. 11, pp. 159–173.
- [4] A. Bhardwaj, L. Sam, Akanksha, F. J. Martín-Torres, and R. Kumar, "UAVs as remote sensing platform in glaciology: Present applications and future prospects," *Remote Sens. Environ.*, vol. 175, pp. 196–204, Mar. 2016.
- [5] D. Leary, "Drones on ice: An assessment of the legal implications of the use of unmanned aerial vehicles in scientific research and by the tourist industry in Antarctica," *Polar Rec.*, vol. 53, no. 4, pp. 343–357, May 2017.
- [6] C. Gaffey and A. Bhardwaj, "Applications of unmanned aerial vehicles in cryosphere: Latest advances and prospects," *Remote Sens.*, vol. 12, no. 6, p. 948, Mar. 2020.
- [7] I. Colomina and P. Molina, "Unmanned aerial systems for photogrammetry and remote sensing: A review," *ISPRS J. Photogrammetry Remote Sens.*, vol. 92, pp. 79–97, Jun. 2014.
- [8] D. Bliakharskii, I. Florinsky, and T. Skrypitsyna, "Modelling glacier topography in antarctica using unmanned aerial survey: Assessment of opportunities," *Int. J. Remote Sens.*, vol. 40, no. 7, pp. 2517–2541, Mar. 2019.
- [9] J. C. Ryan *et al.*, "Derivation of high spatial resolution albedo from UAV digital imagery: Application over the Greenland ice sheet," *Frontiers Earth Sci.*, vol. 5, pp. 40–52, May 2017.
- [10] T. Li *et al.*, "Resolving fine-scale surface features on polar sea ice: A first assessment of UAS photogrammetry without ground control," *Remote Sens.*, vol. 11, no. 7, p. 784, Apr. 2019.
- [11] J. Rennie, *Aurora australis uses drone technology to navigate sea ice*. Australian Antarctic Division-News and Media, Dec. 2015. [Online]. Available: <http://www.antarctica.gov.au/news/2015/aurora-australis-uses-drone-tech-nology-to-navigate-sea-ice>
- [12] R. O. R. Jenssen, M. Eckerstorfer, and S. Jacobsen, "Drone-mounted ultrawideband radar for retrieval of snowpack properties," *IEEE Trans. Instrum. Meas.*, vol. 69, no. 1, pp. 221–230, Jan. 2020.
- [13] M. Korczak-Abshire, A. Zmarz, M. Rodzewicz, M. Kycko, I. Karsznia, and K. J. Chwedorzewska, "Study of fauna population changes on Penguin Island and Turret Point Oasis (King George Island, Antarctica) using an unmanned aerial vehicle," *Polar Biol.*, vol. 42, no. 1, pp. 217–224, Jul. 2018.
- [14] V. Miranda, P. Pina, S. Heleno, G. Vieira, C. Mora, and C. E. Schaefer, "Monitoring recent changes of vegetation in Fildes peninsula (King George Island, Antarctica) through satellite imagery guided by UAV surveys," *Sci. Total Environ.*, vol. 704, Feb. 2020, Art. no. 135295.
- [15] C. Leuschen *et al.*, "UAS-based radar sounding of the polar ice sheets," *IEEE Geosci. Remote Sens. Mag.*, vol. 2, no. 1, pp. 8–17, Mar. 2014.
- [16] G. Joutet *et al.*, "Short-lived ice speed-up and plume water flow captured by a VTOL UAV give insights into subglacial hydrological system of Bowdoin glacier," *Remote Sens. Environ.*, vol. 217, pp. 389–399, Nov. 2018.

- [17] C. Jones, J. Ryan, T. Holt, and A. Hubbard, "Structural glaciology of Isunguata Sermia, West Greenland," *J. Maps*, vol. 14, no. 2, pp. 517–527, Aug. 2018.
- [18] A. Bhardwaj, L. Sam, A. Bhardwaj, and F. J. Martín-Torres, "LiDAR remote sensing of the cryosphere: Present applications and future prospects," *Remote Sens. Environ.*, vol. 177, pp. 125–143, May 2016.
- [19] J. R. Mertes, J. D. Gulley, D. I. Benn, S. S. Thompson, and L. I. Nicholson, "Using structure-from-motion to create glacier DEMs and orthoimagery from historical terrestrial and oblique aerial imagery," *Earth Surf. Process. Landforms*, vol. 42, no. 14, pp. 2350–2364, Jul. 2017.
- [20] A. Köhler, M. Petlicki, P.-M. Lefeuvre, G. Buscaino, C. Nuth, and C. Weidle, "Contribution of calving to frontal ablation quantified from seismic and hydroacoustic observations calibrated with LiDAR volume measurements," *Cryosphere*, vol. 13, no. 11, pp. 3117–3137, Nov. 2019.
- [21] N. Putkinen *et al.*, "High-resolution LiDAR mapping of glacial landforms and ice stream lobes in finland," *Bull. Geological Soc. Finland*, vol. 89, no. 2, pp. 64–81, Dec. 2017.
- [22] P.-A. Duviollard, L. Ravelin, P. Deline, and L. Dubois, "Paraglacial rock slope adjustment beneath a high mountain infrastructure—The Pilatte hut case study (Écrins mountain range, France)," *Frontiers Earth Sci.*, vol. 6, pp. 94–107, Jul. 2018.
- [23] R. I. Crocker, J. A. Maslanik, J. J. Adler, S. E. Palo, U. C. Herzfeld, and W. J. Emery, "A sensor package for ice surface observations using small unmanned aircraft systems," *IEEE Trans. Geosci. Remote Sens.*, vol. 50, no. 4, pp. 1033–1047, Apr. 2012.
- [24] R. Huang, L. Jiang, H. Wang, and B. Yang, "A bidirectional analysis method for extracting glacier crevasses from airborne LiDAR point clouds," *Remote Sens.*, vol. 11, no. 20, p. 2373, Oct. 2019.
- [25] M. Mellor, "Antarctic ice terminology: Ice dolines," *Polar Rec.*, vol. 10, no. 64, pp. 92–92, Jan. 1960.
- [26] J. Moore, "Ice blisters and ice dolines," *J. Glaciology*, vol. 39, no. 133, pp. 714–716, Feb. 1993.
- [27] K. A. Krebs, "The morphology and dynamics of the lower Lambert glacier and Amery ice shelf system," Jan. 1997. [Online]. Available: https://eprints.utas.edu.au/20418/7/whole_KrebsKimA1998.pdf
- [28] R. Bindschadler, T. A. Scambos, H. Rott, P. Skvarca, and P. Vornberger, "Ice dolines on Larsen ice shelf, Antarctica," *Ann. Glaciol.*, vol. 34, pp. 283–290, 2002.
- [29] I. V. Florinsky and D. P. Bliakharskii, "The 2017 catastrophic subsidence in the Dalk glacier, East Antarctica: Unmanned aerial survey and terrain modelling," *Remote Sens. Lett.*, vol. 10, no. 4, pp. 333–342, Jan. 2019.
- [30] D. Turner, A. Lucieer, and C. Watson, "An automated technique for generating georectified mosaics from ultra-high resolution unmanned aerial vehicle (UAV) imagery, based on structure from motion (SfM) point clouds," *Remote Sens.*, vol. 4, no. 5, pp. 1392–1410, May 2012.
- [31] T. R. Chudley, P. Christoffersen, S. H. Doyle, A. Abellan, and N. Snooke, "High-accuracy UAV photogrammetry of ice sheet dynamics with no ground control," *Cryosphere*, vol. 13, no. 3, pp. 955–968, Mar. 2019.
- [32] G. Jouvét, Y. Weidmann, E. van Dongen, M. P. Lüthi, A. Vieli, and J. C. Ryan, "High-endurance UAV for monitoring calving glaciers: Application to the Inglefield Bredning and Eqip Sermia, Greenland," *Frontiers Earth Sci.*, vol. 7, pp. 206–220, Aug. 2019.
- [33] J. M. Wheaton, J. Brasington, S. E. Darby, and D. A. Sear, "Accounting for uncertainty in DEMs from repeat topographic surveys: Improved sediment budgets," *Earth Surf. Process. Landforms*, vol. 35, no. 2, pp. 136–156, Feb. 2010.
- [34] S. Ai *et al.*, "High-precision ice-flow velocities from ground observations on Dalk glacier, Antarctica," *Polar Sci.*, vol. 19, pp. 13–23, Mar. 2019.
- [35] A. Xie, S. Wang, Y. Wang, and C. Li, "Comparison of temperature extremes between Zhongshan station and Great Wall station in Antarctica," *Sci. Cold Arid Regions*, vol. 10, no. 5, pp. 369–378, Nov. 2018.
- [36] G. Jozkow, C. Toth, and D. Grejner-Brzezinska, "UAS Topographic mapping with Velodyne LiDAR sensor," *ISPRS Ann. Photogrammetry Remote Sens. Spatial Inform. Sci.*, vol. III-1, pp. 201–208, Jun. 2016.
- [37] M. Westoby, J. Brasington, N. Glasser, M. Hambrey, and J. Reynolds, "'Structure-from-motion' photogrammetry: A low-cost, effective tool for geoscience applications," *Geomorphology*, vol. 179, pp. 300–314, Dec. 2012.
- [38] M. A. Fonstad, J. T. Dietrich, B. C. Courville, J. L. Jensen, and P. E. Carbonneau, "Topographic structure from motion: A new development in photogrammetric measurement," *Earth Surf. Process. Landforms*, vol. 38, no. 4, pp. 421–430, Jan. 2013.
- [39] M. R. James, S. Robson, and M. W. Smith, "3-D uncertainty-based topographic change detection with structure-from-motion photogrammetry: Precision maps for ground control and directly georeferenced surveys," *Earth Surf. Process. Landforms*, vol. 42, no. 12, pp. 1769–1788, Mar. 2017.
- [40] T. Li, Y. Liu, T. Li, F. Hui, Z. Chen, and X. Cheng, "Antarctic surface ice velocity retrieval from MODIS-based mosaic of Antarctica (MOA)," *Remote Sens.*, vol. 10, no. 7, p. 1045, Jul. 2018.
- [41] L. M. Cathles, D. S. Abbot, J. N. Bassis, and D. R. MacAyeal, "Modeling surface-roughness/solar-ablation feedback: Application to small-scale surface channels and crevasses of the Greenland ice sheet," *Ann. Glaciol.*, vol. 52, no. 59, pp. 99–108, 2011.
- [42] S. Gindraux, R. Boesch, and D. Farinotti, "Accuracy assessment of digital surface models from unmanned aerial vehicles' imagery on glaciers," *Remote Sens.*, vol. 9, no. 2, p. 186, Feb. 2017.
- [43] P. Passalacqua *et al.*, "Analyzing high resolution topography for advancing the understanding of mass and energy transfer through landscapes: A review," *Earth Sci. Rev.*, vol. 148, pp. 174–193, Sep. 2015.
- [44] W. Li, K. Sun, D. Li, T. Bai, and H. Sui, "A new approach to performing bundle adjustment for time series UAV images 3D building change detection," *Remote Sens.*, vol. 9, no. 6, p. 625, Jun. 2017.
- [45] M. V. Peppas, J. P. Mills, P. Moore, P. E. Miller, and J. E. Chambers, "Automated co-registration and calibration in SfM photogrammetry for landslide change detection," *Earth Surf. Process. Landforms*, vol. 44, no. 1, pp. 287–303, Oct. 2018.
- [46] K. L. Cook and M. Dietze, "Short communication: A simple workflow for robust low-cost UAV-derived change detection without ground control points," *Earth Surf. Dyn.*, vol. 7, no. 4, pp. 1009–1017, Oct. 2019.
- [47] D. Lague, N. Brodeur, and J. Leroux, "Accurate 3D comparison of complex topography with terrestrial laser scanner: Application to the Rangitikei canyon (N-Z)," *ISPRS J. Photogrammetry Remote Sens.*, vol. 82, pp. 10–26, Aug. 2013.
- [48] J. Šupinský, J. Kaňuk, Z. Hochmuth, and M. Gallay, "Detecting dynamics of cave floor ice with selective cloud-to-cloud approach," *Cryosphere*, vol. 13, no. 11, pp. 2835–2851, Nov. 2019.
- [49] J. C. Fernandez-Diaz *et al.*, "Early results of simultaneous terrain and shallow water bathymetry mapping using a single-wavelength airborne LiDAR sensor," *IEEE J. Sel. Topics Appl. Earth Observ. Remote Sens.*, vol. 7, no. 2, pp. 623–635, Feb. 2014.



Teng Li received the B.Sc. degree in geographic science from Wuhan University, China, in 2015. He is currently working toward the Ph.D. degree in global environmental change at Beijing Normal University, China.

His research interests include image processing, glacial dynamics, ice sheet mass balance, InSAR, and UAV operation. In the 2017–2018 Chinese Antarctic Expedition, he carried out a glaciology investigation using UAVs in Zhongshan Station of China, East Antarctica.



Baogang Zhang received the B.Sc. degree from the Tongji University, and the M.S. degree from the Institute of Remote Sensing Applications, Chinese Academy of Sciences, Beijing, China, in 2011.

He joined the College of Global Change and Earth System Science, Beijing Normal University, China, as the HPC Administrator and currently is working toward the Ph.D. degree in global environmental change at the same university. His research interests include UAV applications in polar regions, parallel computing, and data processing.



Wen Xiao received the B.S. degree in geodesy and geomatics from the Wuhan University, Wuhan, China, in 2010, the M.S. (cum laude) degree in geoinformatics from ITC, University of Twente, Enschede, The Netherlands, in 2012, and the Ph.D. degree in geoinformation science and technology from IGN, Universit Paris-EST, Paris, France, in 2015.

Since 2016, he has been a Lecturer and University Research Fellow with Newcastle University, Newcastle Upon Tyne, U.K. His research interests include 3D mapping, laser scanning, photogrammetric computer vision, and their applications in urban and natural environments.

Dr. Xiao is a Council Member of RSPSoc.



Zhenhong Li (Senior Member, IEEE) received the B.Sc. degree in geodesy from the Wuhan Technical University of Surveying and Mapping (now Wuhan University), Wuhan, China, in 1997, and the Ph.D. degree in geodesy and navigation from the University College London, London, U.K., in 2005.

He is a Professor of imaging geodesy with the School of Engineering, Newcastle University, Newcastle Upon Tyne, U.K. He has more than 20 years of research experience in space geodesy and remote sensing (mainly InSAR and GNSS) and their application to geohazards (e.g., earthquakes, landslides, and land subsidence) and precision agriculture. He specializes in development of InSAR atmospheric corrections and time-series algorithms for precisely mapping surface movements, and has made several original contributions to the direct estimation and/or mitigation of the effects of atmospheric water vapor on satellite radar measurements.



Xiao Cheng received the M.S. degree in geodesy and measurement engineering from Wuhan University, China, in 2001, and the Ph.D. degree in cartography and geographic information systems from the Chinese Academy of Sciences, Beijing, in 2004.

He is currently a Professor and Dean of the School of Geospatial Engineering and Science, Sun Yat-Sen University. He has authored more than 60 peer-reviewed articles. His research interests include the observation of climate change impacts in polar regions such as ice sheets, ice shelves, and sea ice using remote sensing technology.

Dr. Cheng is the council member of the Chinese National Committee of Polar Experts and the secretary-general of University Corporation for Polar Research (UCPR).



Jian Zhao received the B.Sc. degree in geographic information science from the Hefei University of Technology, in 2015, and the M.S. degree in global environmental change from Beijing Normal University, China, in 2018.

He is currently a Geospatial Engineer with Beijing North-Star Digital Remote Sensing Technology Company, Ltd. His research interests include 3D terrain modeling and change detection.